Laser Spectroscopic and Theoretical Studies of Encapsulation Complexes of Calix[4]arene

Shohei Kaneko,[1] Yoshiya Inokuchi, [1] Takayuki Ebata, [*1], Edoardo Aprà[2]
and Sotiris S. Xantheas[*3*]

[1] Department of Chemistry, Graduate School of Science, Hiroshima University,
Higashi-Hiroshima 739-8526, Japan
[2] Computer Science and Mathematics Division, Oak Ridge National Laboratory,
Oak Ridge, TN 37831, USA
[3] Chemical & Materials Sciences Division, Pacific Northwest National Laboratory,
902 Battelle Boulevard, P.O. Box 999, MS K1-83, Richland, WA 99352, USA

Abstract

The complexes between the host calix[4]arene (C4A) and various guest molecules such as NH_3, N_2, CH_4, and C_2H_2 have been investigated via experimental and theoretical methods. The S_1-S_0 electronic spectra of these guest-host complexes are observed by mass-selected resonant two-photon ionization (R2PI) and laser induced fluorescence (LIF) spectroscopy. The infrared (IR) spectra of the complexes formed in molecular beams are obtained by IR-UV double resonance (IR-UV DR) and IR photodissociation (IRPD) spectroscopy. The supramolecular structures of the complexes are investigated by electronic structure methods (density functional and second order perturbation theory). The current results for the various molecular guests are put in perspective with the previously reported ones for the C4A-Rare Gas (Rg) (*Phys. Chem. Chem. Phys*. **2007**, *126*, 141101) and C4A-H_2O complexes (*J. Phys. Chem*. A, **2010,** *114,* 2967). The electronic spectra of the complexes of C4A with N_2, CH_4 and C_2H_2 exhibit red-shifts of similar magnitudes with the ones observed for the C4A-Rg complexes, whereas the complexes of C4A with H_2O and NH_3 show much larger red-shifts. Most of the IR-UV DR spectra of the complexes, except for C4A-C_2H_2, show a broad hydrogen bonded OH stretching band with a peak at ~3160 cm^{-1}. The analysis of the experimental results, in agreement with the ones resulting from the electronic structure calculations, suggests that C4A preferentially forms endo-complexes with all the guest species reported in this study. We discuss the similarities and differences of the structures, binding energies and the nature of the interaction between the C4A host and the various guest species.

I. Introduction

Calixarenes (CAs) are macrocyclic compounds that are well known as functional molecules in host-guest chemistry. Their structures are comprised of cavities that are formed by phenyl rings connected by methylene and OH groups. The latter are strongly hydrogen-bonded to each other at the lower rim of the molecular cavity. This cavity functions as a molecular receptor and can encapsulate a variety of species through non-covalent interactions, forming various clathrates.[1-4] In addition, CAs have pKa values that are quite different from those of their monomeric units, as a result of the strong hydrogen bonding between the OH groups.[5] Up to now, many previous studies have aimed at establishing the functionality of CAs, such as their molecular recognition, by substituting a variety of groups at the para-position of either the phenyl ring[6] or the OH group[7]. The resulting complex structures are normally studied by NMR and X-ray diffraction methods at room temperature.[8-13] However, the thermal energy at room temperature is often equal to the host-guest interaction energy, especially for the complexes with neutral guest species. This yields very broad or complicated spectra arising from the averaging over all possible conformers at a given temperature. The interaction with solvent molecules will further affect the complex structure. For the full understanding of the intrinsic properties of the host molecules and the details of the nature of the interaction between the host CAs and the guest species, a precise spectroscopic and theoretical study of well-defined complex structures is necessary.

We have previously investigated the structures of the complexes of calix[4]arene (C4A) in the gas phase by a variety of laser spectroscopic methods and by quantum chemical calculations. C4A is the smallest size of CAs in which the molecular host cavity consists of four phenol units. The complexes are generated in a supersonically cooled condition in the gas phase so that the issues related to both thermal fluctuations and solvent effects can be removed. The UV and IR spectra of the specific complexes are measured and the analysis of the molecular geometries and corresponding spectra via high level quantum chemical calculations enables us to determine their supramolecular structures. Using this joint experimental-theoretical approach we have previously reported that the Ar_n clusters are bound to the C4A cavity in C4A-Ar_n complexes[14], and that the C4A-H_2O complex has an endo- structure (water inside the C4A cavity), thus forming the "World's

smallest cup of water" [15].

In the present study we report the structures of the complexes of C4A with variety of neutral guest species, namely CH_4, N_2, C_2H_2 and NH_3. These guests were chosen because they can be bound to the C4A host via different interactions, such as dispersion, CH-π hydrogen-bonding and dipole-dipole interactions. We examine how the different nature of the guest/host interaction affects the encapsulation structure, the electronic transition energy and the total binding energy. For this purpose we apply several laser spectroscopic methods and electronic structure calculations at various levels of theory.

II. Approach

Experimental Details: Jet cooled C4A is generated by an adiabatic expansion of the sample vapor diluted with Ne or He carrier gas. Since C4A is a nonvolatile molecule, we used a high temperature pulse nozzle.[16] C4A in its powder form was introduced in a housing at the top of the pulsed nozzle heated at 140^{o}C and the gaseous mixture with carrier gas at the total pressure of 2 bar was subsequently expanded into the vacuum through a 2mm aperture of the nozzle. The free jet was skimmed by a skimmer located at 40 mm downstream of the nozzle, forming a supersonic beam. The C4A complexes were formed by using a premixed guest/Ne as the carrier gas. C4A and its complexes in the beam cross with the UV or IR laser light at 50 mm downstream of the skimmer. The UV spectra are measured by either mass-selected resonant two-photon ionization (R2PI) or laser induced fluorescence (LIF) spectroscopy. The IR spectrum of each species is measured by IR-UV double resonance (DR) spectroscopy or IR photodissociation (IRPD) spectroscopy. Excitation schemes for the IR-UV DR and IRPD spectroscopy are shown in Figure 1. For the R2PI measurement the ions are extracted into a time-of-flight (TOF) tube with a length of 50 cm and are detected by a channeltron (Burlei 4900). The ion current is monitored by a digital oscilloscope and the signal is processed by a boxcar integrator (Stanford Research Systems SR245) connected to a personal computer.

A tunable UV laser light is obtained by a second harmonic (Inrad Autotracker Ⅲ/BBO crystal) of the Nd:YAG laser pumped dye laser (Continuum Surelite Ⅱ/Lambda Physique

Scanmate). A tunable IR laser light is generated by Nd:YAG laser pumped optical parametric oscillator (Quanta-Ray, GCR250 / laser Vision). The typical power and spectral resolution of the tunable IR light are 5 mJ and 1 cm^{-1}, respectively. For the measurement of the IR-UV DR spectra the IR laser pulse is introduced coaxially to the UV probe laser at 110 ns prior to the probe UV pulse. When the population of probed species monitored by the UV laser is pumped to the upper vibrational level, the monitored signal decreases and we obtain the IR spectrum as a fluorescence-dip or ion-dip spectrum. In the measurement of the IRPD spectrum the UV laser frequency is fixed to a few wavenumbers on the lower frequency side of the (0,0) band of bare C4A and the population of the C4A fragment is monitored. When the vibrational excitation energy is larger than the corresponding binding energy, the complex dissociates via vibrational predissociation and generates the C4A fragment. Therefore, by scanning the IR frequency while monitoring the C4A fragment, we obtain the photofragment detected IR photodissociation (IRPD) spectrum. The dissociation energy of the complex can be determined by comparing the IR dip and IRPD spectra. C4A (98%) was purchased from Tokyo Chemical Industry Co. and was used without further purification.

Theoretical calculations: The stable structures and binding energies of the complexes were determined at various levels of electronic structure theory. DFT calculations were initially performed at the M05-2X/6-31+G*level using the GAUSSIAN 09 program package[17]. The used M05-2X density functional includes van der Waals interactions and its performance was previously discussed by Zhao and Truhler.[18] Additional first principles calculations were performed at the second order Moller-Plesset (MP2) level of theory[19] using the family of augmented correlation consistent basis sets of Dunning and co-workers[20,21] up to quadruple-zeta quality, aug-cc-pV*n*Z (*n* = D, T, Q). The MP2/aug-cc-pVDZ optimal geometries were used for single point calculations with the larger basis sets up to aug-cc-pVQZ. These calculations were performed with the NWChem suite of electronic structure codes[22] at Pacific Northwest National Laboratory. The MP2/aug-cc-pVDZ harmonic vibrational frequencies were scaled by a factor of 0.96, whereas the DFT ones were scaled by a factor of 0.93 in order to better reproduce the observed IR spectra.

The binding energy of the C4A-(M) supramolecular complex is computed as:

(1)

where M denotes the guest species, superscripts denote basis sets and subscripts indicate the geometries of the individual species identified in parentheses, viz. . In this notation, for example, denotes the energy of C4A at the dimer [C4A-(M)] geometry with the monomer (C4A) basis set.

The basis set superposition error (BSSE) correction was estimated via the function counterpoise (fCP) method[23] that includes the fragment relaxation terms[24], which arise from the change in the intramolecular geometry of the C4A and M fragments in the complex minimum. Using the same notation introduced previously, the BSSE-corrected dimer binding energies are:

(2)

where

(3a)

(3b)

are the fragment relaxation terms. Therefore, 4 additional calculations (C4A and M with the full complex basis at the complex and at the isolated MP2/aug-cc-pVDZ geometries) are required for each BSSE calculation.

III. Results and Discussion

III.1. Electronic spectra

Figure 2 shows the S_1 - S_0 R2PI spectra of (a) C4A, (b) C4A-Ar, (c) C4A-N_2, (d) C4A-CH_4, (e) C4A-C_2H_2, (f) C4A-H_2O and (g) C4A-NH_3. All the spectra exhibit weak band origins and strong vibronic bands located ~170 cm^{-1} above the origins. The appearance of these strong bands is due to the vibronic coupling with a dipole-allowed S_2 ($^1E_2$) state under C_4 symmetry. The band origin of the bare C4A (Fig. 1(a)) is located at 35357 cm^{-1} and the one of C4A-Ar (Fig. 2(b)) is red-shifted by 45 cm^{-1} with respect to the bare C4A. The electronic spectrum of C4A-Ar exhibits

a spectral pattern that is very similar with the one for bare C4A. In our previous work[25] we have determined that the C4A-Ar complex forms an endo- structure of C_4 symmetry, in which the Ar atom is located inside the C4A cavity lying along the C_4 axis of C4A.[25] For the C4A-N_2 complex a sharp band origin at 35292 cm^{-1} is observed, which is shifted by 65 cm^{-1} from that of bare C4A. The overall spectral pattern is very similar with that of bare C4A, a fact suggesting that this complex also has C_4 symmetry.

The spectral features of the C4A-CH_4 (Fig. 2d) and C4A-C_2H_2 (Fig. 2e) complexes are different from those for C4A-Ar and/or C4A-N_2. The spectra of C4A-CH_4 exhibit a very weak band origin at 35289 cm^{-1} and a strong band at 35470 cm^{-1}. To confirm that the weak band at 35289 cm^{-1} is the band origin, and to further examine the possibility of other isomers in the spectra, we measured the UV-UV HB spectrum of the complex by monitoring the band at 35470 cm^{-1}, which is marked by an asterisk in Fig. 2(d). The obtained UV-VU HB spectrum is shown at the lower panel of Fig. 2(d). The UV-UV HB spectrum shows essentially the same structure with that of the R2PI, though the bands of the former are sharper than those of the latter. We therefore conclude that only one isomer is present in the spectrum and the position of the band origin is at 35289 cm^{-1}. The spectrum of C4A-C_2H_2 shows a sharp band origin at 35273 cm^{-1}, which is red-shifted by 84 cm^{-1} with respect to that of bare C4A. However, the intervals of the vibronic bands with respect to the band origin have a different pattern from those of bare C4A and the C4A-Ar, C4A-N_2 complexes. The difference in the vibronic pattern can be attributed to the lowering of the symmetry due to the distortion of the C4A cavity as a result of the encapsulation of the guest (*vide infra*). Table 1 lists the frequencies of the S_1 - S_0 band origin for the various complexes and the red-shifts with respect to the band origin of bare C4A. Figure 3 shows the plots of the red-shifts of the band origin of the complexes from that of bare C4A as a function of the polarizability of the guest species. The shifts for the C4A-N_2, C4A-CH_4 and C4A-C_2H_2 complexes lie close to the trend defined by the monotonic change in the C4A-Rg (Rg=Ne, Ar, Kr, Xe) series. In contrast, the shifts of the C4A-H_2O and C4A-NH_3 complexes show more complicated vibronic structures than the others and are associated with much larger red shifts (~200 cm^{-1}) from the C4A-Rg series. These large shifts can be attributed to the large dipole moments of

the guests. The band origins of C4A-H_2O (Fig. 2f) and C4A-NH_3 (Fig. 2g) appear at 35151 and, 35142 cm^{-1}, respectively, yielding red-shifts of 206 and 215 cm^{-1}. In addition, a progression with an interval of 4 cm^{-1} appears in the spectrum of C4A-NH_3. The structure of the low frequency vibronic bands is more complicated in C4A-H_2O (Fig. 2f). All these low frequency bands can be related to the internal motion of the guest species inside the cavity.

III.2. IR-UV DR and IRPD spectra

The left panel of Fig. 4 shows the IR-UV DR spectrum of C4A (Fig. 4(a)) and the C4A-N_2 complex (Fig. 4b). The calculated IR spectra of the two lowest energy complexes, whose structures are given in Figure 7, are shown in Figures 4(c) and 4(d). The IR-UV DR spectra of both C4A and C4A-N_2 exhibit a broad H-bonded OH stretch band centered at 3160 cm^{-1} and several CH stretch bands in the 2800-3000 cm^{-1} region. For C4A the band at 3160 cm^{-1} is attributed to the degenerate hydrogen-bonded OH stretching vibration of the phenolic OH groups under C_4 symmetry. The invariance of the H-bonded OH stretching band indicates that the H-bonded structure of the phenolic OH groups at the lower rim is not affected by the complexation with N_2.

The right panel of Fig. 4 shows the IR-UV DR spectrum of C4A-CH_4 (Fig. 4(f)), which is also very similar to that of bare C4A (Fig. 4(e)). The calculated IR spectra of that complex, whose structure is shown in Fig. 7, is shown in Fig. 4(g).

Fig. 5(b) shows the IR spectrum of C4A-C_2H_2. For this complex we could not obtain the IR-UV DR spectrum, so that only the IRPD spectrum is shown. The IR spectrum of C4A-C_2H_2 shows two bands at 3160 and 3190 cm^{-1}, both of which are assigned to the H-bonded OH stretching vibrations. The width of the higher frequency band is narrower and its intensity is weaker than the one for the lower frequency band. The calculated spectra for the two energy complexes of C4A-C_2H_2, whose structures are given in Figure 7, are shown in Figs. 5(c) and 5(d). For comparison, the IR-UV DR spectrum of C4A is shown in Fig. 5(a). As to the binding energy, we can estimate its upper limit to be 2850 cm^{-1} from the appearance of this band in the IRPD spectrum.

The IR-UV double resonance (DR) spectrum and IRPD spectra of the C4A-NH_3 complex are shown in Figures 6(b) and 6(e). Both the IR-UV DR and IRPD spectra exhibit broad IR bands

with the peak at 3160 cm^{-1} being similar to the one obtained for C4A-Ar, C4A-N_2 and C4A-CH_4. In the lower frequency region several bands are assigned to the CH stretching vibrations. The observed IR spectra indicate that all complexes have endo-structures (guest inside the C4A host cavity). The comparison between the IRPD and IR-UV DR spectra provide additional information about the binding energies of the complexes.[15] When we compare the IRPD and IR-UV DR spectra of the C4A-NH_3 complex, we observe that all bands appearing in the IRPD spectrum coincide with those in the IR-UV DR spectrum. This suggests that the dissociation energy of the C4A-NH_3 complex is lower than the energy region investigated, and we can only provide an upper limit for the dissociation energy at 2810 cm^{-1}, which is the lowest frequency band in this region. The spectra shown in Figs. 6(c) and 6(d) are the ones obtained for the optimized structures of this complex, to be discussed in the next section.

III. 3. Structures of the complexes of C4A

C4A-N_2: We carried initial DFT at the M05-2X/6-31+G* level and subsequent MP2/aug-cc-pVDZ optimizations in order to obtain the stable structures of the complexes of C4A. For C4A-N_2 we obtained two lowest energy endo-complex structures, as shown in Figure 7: (a) a *parallel* (N_2 parallel to the 4-fold axis of C4A retaining C_4 symmetry) and (b) a *perpendicular* complex (N_2 perpendicular to the 4-fold axis). Their relative stabilities, listed in Table 2, suggest that the parallel isomer is more stable at both the DFT and MP2 levels of theory. However, DFT seems to underestimate the energy separation between the parallel/perpendicular isomers by about a factor of 3 when compared to MP2 (9.95 kJ/mol). The larger stability of the parallel isomer is due to the dipole-induced-dipole interaction between C4A and N_2, which is missing in the perpendicular one. Because the overall C_4 symmetry is retained in the parallel isomer, the observed UV spectrum shows very similar features with that of the bare C4A as well as C4A-Ar. In addition, the calculated IR spectrum of the parallel isomer shows a single OH stretching band, while the IR spectrum of the perpendicular isomer shows a doublet structure, because the symmetry is reduced to C_2 in that case. The calculated IR spectrum of parallel isomer is in good agreement with the observed one, and we therefore assign the structure of the parallel endo isomer to the observed

C4A-N_2 complex.

C4A-CH_4: The structure of the endo isomer of C4A-CH_4 at the MP2/aug-cc-pVDZ level is shown in Figure 7 (c). In this complex, one CH group is oriented along the 4-fold axis and points to the bottom of the C4A host. As regards the other three CH groups, two of them are pointing towards the phenyl rings forming weak CH—π hydrogen bonding. This structure could not be converged at the M05-2X/6-31+G* level because of the very low barrier of the internal rotation of CH_3 along the four-fold C4A axis. In this arrangement, the OH stretching vibrations of the host C4A are thought to be almost unaffected by the complexation with CH_4. Indeed, the observed IR spectrum is very similar to that of bare C4A, a fact that is consistent with this structure. Since the complex does not retain the C_4 point group symmetry, the observed UV spectrum exhibits complicated structure.

C4A-C_2H_2: Both the M05-2X/6-31+G* and MP2/aug-cc-pVDZ optimizations yield two stable structures, shown in Figure 7, namely an endo (Fig. 7(d)) and an exo isomer (Fig. 7(e)). The endo is more stable by 48.19 kJ/mol than the exo isomer at the MP2 level of theory. As for the case of the C4A-N_2 complex, DFT was found to severely underestimate the energy difference between the two isomers by a factor of 2.5 when compared to MP2. In the most stable endo isomer the acetylene molecule lies perpendicular to the 4-fold axis and is bound to the phenyl rings via CH-π H-bonding (endo-perpendicular arrangement). No stable structure of the endo-parallel arrangement (C_2H_2 along the 4-fold axis of C4A) could be located.

In the endo-perpendicular arrangement the frame of the C4A host is distorted and the overall symmetry is reduced to C_2. This causes the degenerate OH stretching band of C4A to split into two bands at 3130 and 3205 cm^{-1}. In the observed IRPD spectrum we also identified two bands at 3160 and 3190 cm^{-1}, which coincide to the two OH stretching bands. These results further confirm that the observed C4A-C_2H_2 complex has the endo-perpendicular arrangement, shown in Figure 7(d). We could not identify the asymmetric CH stretching vibration of acetylene due to the overlap of the broad OH stretching vibrations.

C4A-NH_3: The two stable structures of the C4A-NH_3 complex corresponding to the endo and exo isomers are shown in Figures 7(f) and 7(g), respectively. In the exo isomer NH_3 is incorporated in the H-bonding network of the phenolic OH groups, while in the endo isomer it lies inside the C4A cavity with the N atom directed to the lower rim. The endo isomer is 34.57 kJ/mol more sable than the exo isomer at the MP2/aug-cc-pVDZ level (cf. Table 2). DFT does predict the correct order but it again underestimates the energy separation between the two by almost a factor of 3 when compared to MP2. The calculated IR spectrum of the endo isomer exhibits an intense H-bonded OH band at 3160 cm^{-1}, while the exo isomer has four distinct OH stretching bands. It is clear that the calculated IR spectrum of the endo isomer is in better agreement with the observed IR spectrum. We can therefore conclude that the observed C4A-NH_3 complex has the endo structure of Fig. 7(f).

The arrangement of the most stable endo isomer of the C4A-NH_3 complex is similar to that of the most stable endo C4A-H_2O complex, in which a water molecule is encapsulated in the C4A cavity with the oxygen atom pointing towards the lower rim of C4A. A common characteristic in the two complexes is that the guest species have permanent dipole moments; the dipole moment of a water molecule is 1.855 Debye[26] and that of an ammonia molecule is 1.472 Debye[26]. In addition, the dipole moment of C4A is calculated to be 2.312 Debye. The endo arrangement of both complexes arises from the dipole-dipole alignment between the host C4A and the guest species. Thus the complexes are stabilized mainly by the dipole-dipole interaction between the host and guest in addition to the dispersion forces. The calculated dipole moments are 3.434 and 3.273 Debye for the C4A-H_2O and C4A-NH_3 complexes, respectively. The stabilization of the complexes by mainly the dipole-dipole interaction is consistent with the experimental estimates for the upper limits of their binding energies. These are 2810 cm^{-1} for C4A-NH_3 and 3140 cm^{-1} C4A-H_2O,[15] a difference that can be attributed to the smaller dipole moment of NH_3 when compared to H_2O as well as the smaller dipole moment of the C4A-NH_3 complex (3.273 D) when compared to that of the C4A-H_2O complex (3.434 D).

IV. Binding energies of the C4A-M complexes

The previous analysis suggests that all C4A-M complexes considered in this study form endo isomers, in which the guest species (M) are encapsulated inside the C4A cavity. The binding energies for the various guests are different, since the nature of the major interaction between with the host varies for the different guests, as also evidenced from the variation of the corresponding red shift of the S_1-S_0 transition versus the polarizability of the guest species shown in Figure 3. The binding energies of the complexes calculated at the MP2/aug-cc-pV*n*Z (*n* = D, T, Q) level of theory are listed in Table 3. The CCSD(T)/aug-cc-pVDZ binding energies for M=Ar, H_2O and NH_3 are shown in parentheses. The Table includes the results for the H_2O and Ar hosts reported earlier[15,25] for completeness. Estimates of the Complete Basis Set (CBS) limit at the MP2 level using the heuristic extrapolation formula $A + B \exp(C\, n^2)$, where *n* is the cardinal number (*n*=2, 3, 4) of the aug-cc-pV*n*Z basis set and *A*, *B* and *C* are constants (*A* is the CBS limit) are also listed. The complexes of C4A with the -CH_4, -H_2O and -N_2 hosts have similar (within 2.5 kJ/mol) binding energies. The binding energy of the C4A-NH_3 complex is predicted to be larger than that of C4A-H_2O at both the MP2 and CCSD(T) levels of theory. With the smaller aug-cc-pVDZ basis set MP2/CCSD(T) predicts the binding energy of C4A-NH_3 to be 15.5/11.0 kJ/mol larger than that of C4A-H_2O; at the MP2/CBS limit this difference is 12.6 kJ/mol. Although the dipole-dipole interaction for the former is smaller than that of the later (as the permanent dipole moment of NH_3 is ~80% than that of H_2O), the three NH-π interactions in C4A- NH_3 stabilize this complex more than the two OH-π interactions present in C4A-H_2O.

Finally the MP2/CBS results yield the largest binding energy (53.56 kJ/mol) for C4A-C_2H_2, arising from the CH-π H-bonding in addition to the dispersion interaction. The IRPD measurement again suggests a smaller binding energy than that predicted from the calculations. Since the IRPD measurement covers a limited energy region of the nonlinear optics and the number of IR active bands, a different experiment such as SEP, which can cover a wider energy region, will be necessary in the future to determine a more precise threshold for the binding energy.

V. Conclusions

The structures of complexes of the host C4A with various guest species, namely Ar, N_2,

CH_4 C_2H_2, H_2O and NH_3, have been investigated by experimental LIF, R2PI, IR-UV double resonance and IR photodissociation spectroscopy and by high-level quantum chemical calculations. For all molecular guests considered in this study, it was determined that the supramolecular complex assumes an endo arrangement (guest inside the cavity of the C4A host). The complexes can be further classified into two groups based on the magnitude of the red-shift of the S_1-S_0 electronic transition with respect to that of bare C4A. The first group, consisting of the -H_2O and -NH_3 guests, exhibits red shifts that are as large as 200 cm^{-1}; the second group, consisting of the -Ar, -N_2, -CH_4 and -C_2H_2 guests, shows rather small (10-80 cm^{-1}) red-shifts, which vary roughly proportional with the polarizability of the guest species. It is suggested that the complexes belonging to the first group are bound mainly by dipole-dipole interactions, while the ones in the second group are bound mainly by dispersion forces. For the C4A-C_2H_2 complex, CH-π hydrogen bonding is an additional factor contributing to its stabilization. For most complexes, the IR-UV DR spectra show a strong and broad H-bonded phenolic OH stretching band centered at 3160 cm^{-1}. The spectrum of C4A-C_2H_2 is the exception, showing a doublet structure for the OH stretching band due to the deformation of the ring upon the encapsulation of C_2H_2 by the host C4A. Estimates of the binding energies of the complexes, obtained at the MP2/CBS level, suggest the following order for the various hosts: Ar, CH_4, H_2O, N_2, NH_3, C_2H_2 with the CH_4, H_2O and N_2 hosts having binding energies within 2.5 kJ/mol. Calculations at the CCSD(T) level confirm that the binding energy of the C4A-H_2O complex is smaller than that of the C4A-NH_3 complex. In general, the CCSD(T) binding energies for M=Ar, H_2O, NH_3 are between 80-88% of the corresponding ones obtained at the MP2 level.

Acknowledgments: SSX acknowledges a Fellowship from JSPS for a short visit to the University of Hiroshima. TE acknowledges support from the Japan Society for the Promotion of Science (JSPS) through a Grant-in-Aid project (No. 18205003) and from MEXT through a Grant-in-Aid for the Scientific Research on Priority Area "Molecular Science for Supra Functional Systems" (No. 477). Part of this work was supported by the Chemical Sciences, Geosciences, and Biosciences Division, Office of Basic Energy Sciences, U.S. Department of Energy. Battelle operates the

Pacific Northwest National Laboratory for the U.S. Department of Energy. This research was performed in part using the Molecular Science Computing Facility (MSCF) in the Environmental Molecular Sciences Laboratory, a national scientific user facility sponsored by the Department of Energy's Office of Biological and Environmental Research.

References

(1) Gutsche, C. D. Calixarenes. In *Monographss in Supramolucular Chemistry*; Stoddart, J. F. Ed.; Royal Society of Chemistry: Cambridge, U.K., 1989.

(2) Cram, D. J.; Cram, J. M. Container molecules and their guests. In *Monographss in Supramolucular Chemistry*; Stoddart, J. F., Ed.; Royal Society of Chemistry: Cambridge, U.K., 1994.

(3) Gutsche, C. D. Calixarenes revisited. In *Monographss in Supramolucular Chemistry*; Stoddart, J. F., Ed.; Royal Society of Chemistry: Cambridge, U.K., **1998**.

(4) Gutsche, C. D.; Bauer, L. *J. Am. Chem. Soc.* **1985**, *107*, 6063.

(5) Araki, K.; Iwamoto, K.; Shinkai, S.; Matsuda, T. *Bull. Chem. Soc. Jpn.* **1990**, *63*, 3480.

(6) Benevelli, F.; Kolodziejski, W.; Wozniak, K.; Klinowski, J. *Phys. Chem. Phys.* **2001**, *3*, 1762-1768.

(7) Buscemi, S.; Pace, A.; Piccionello, P. A.; Pappalardo, S.; Garozzo, D.; Pilati, I.; Parisi, F. M. *Tetrah. Lett.* **2006**, *47*, 9049-9052.

(8) Benevelli, F.; Kolodziejski, W.; Wozniak, K.; Klinowski, J. *Chem. Phys. Lett.* **1999**, *308*, 65–70.

(9) Atwood, J. L, Hamada, F.; Robinson, K. D.; Orr, G. W.; Vincent, R. L. *Nature*, **1991**, *349*, 683

(10) Benevelli, F.; Kolodziejski, W.; Wozniak, K.; Klinowski, J. *Chem. Phys. Lett.* **1999**, *308*, 65.

(11) Molins, M. A.; Nieto, P. M.; Sanchez, C.; Prados, P.; Mendoza, J. De.; Pons, M. *J. Org. Chem.* **1992**, *57*, 6924.

(12) Kuzmicz, R.; Dobrzycki, L.;Wozniak, K.; Benevelli, F.; Klinowski, J.; Kolodziejski, W. *Phys. Chem. Chem. Phys.* **2002**, *4*, 2387.

(13) Young Lag Cho, Dmitry M. Rudkevich, Alexander Shivanyuk, Kari Rissanen, and Julius Rebek, Jr. *Chem. Eur. J.* **2000**, *6*, No. 20.

(14) Ebata, T.; Hodono, Y.; Ito, T.; Inokuchi, Y. *J. Chem. Phys.* **2007**, *126*, 141101.

(15) Hontama, N.; Inokuchi, Y.; Ebata, T.; Dedonder-Lardeux, C.; Jouvet, C.; Xantheas, S. S. *J. Phys. Chem. A* **2010,** *114,* 2967–2972.

(16) Demchuk, A.; Porter, J.; Koplitz, B . *J.Phys. Chem. A.,* **1998**, *102*, 8841-8846.

(17) Frisch, M. J.; Trucks, G. W.; Schlegel, H. B.; Scuseria, G. E.; Robb, M. A.; Cheeseman, J. R.; Scalmani, G.; Barone, V.; Mennucci, B.; Petersson, G. A.; Nakatsuji, H.; Caricato, M.; Li, X.; Hratchian, H. P.; Izmaylov, A. F.; Bloino, J.; Zheng, G.; Sonnenberg, J. L.; Hada, M.; Ehara, M.; Toyota, K.; Fukuda, R.; Hasegawa, J.; Ishida, M.; Nakajima, T.; Honda, Y.; Kitao, O.; Nakai, H.; Vreven, T.; Montgomery, J. A., Jr.; Peralta, J. E.; Ogliaro, F.; Bearpark, M.; Heyd, J. J.; Brothers, E.; Kudin, K. N.; Staroverov, V. N.; Kobayashi, R.; Normand, J.; Raghavachari, K.; Rendell, A.; Burant, J. C.; Iyengar, S. S.; Tomasi, J.; Cossi, M.; Rega, N.; Millam, J. M.; Klene, M.; Knox, J. E.; Cross, J. B.; Bakken, V.; Adamo, C.; Jaramillo, J.; Gomperts, R.; Stratmann, R. E.; Yazyev, O.; Austin, A. J.; Cammi, R.; Pomelli, C.; Ochterski, J. W.; Martin, R. L.; Morokuma, K.; Zakrzewski, V. G.; Voth, G. A.; Salvador, P.; Dannenberg, J. J.; Dapprich, S.; Daniels, A. D.; Farkas, O.; Foresman, J. B.; Ortiz, J. V.; Cioslowski, J.; Fox, D. J. Gaussian 09, revision A.02; Gaussian, Inc.: Wallingford, CT, 2009

(18) Zhao, Y.; Truhlar, G. D. *J. Chem. Theory Comput.,* **2006**, *2,* 1009

(19) Møller, C.; Plesset, M. S. *Phys. Rev*. **1934**, *46*, 618.

(20) Dunning, T. H., Jr. *J. Chem. Phys*. **1989**, *90*, 1007.

(21) Kendall, R.; Dunning, T., Jr.; Harrison, R. *J. Chem. Phys*. **1992**, *96*, 6769.

(22) Kendall, R. A.; Apra`, E.; Bernholdt, D. E.; Bylaska, E. J.; Dupuis, M.; Fann, G. I.; Harrison, R. J.; Ju., J.; Nichols, J. A.; Nieplocha, J.; Straatsma, T. P.; Windus, T. L.; Wong, A. T. Comput. Phys. Commun. 2000, 128, 260–283. High Performance Computational Chemistry Group. NWChem, A Computational Chemistry Package for Parallel Computers, version 4.6; Pacific Northwest National Laboratory: Richland, WA 99352, 2003.

(23) Boys, S. F.; Bernardi, F. *Mol. Phys*. **1970**, *19*, 55.

(24) Xantheas, S. S. *J. Chem. Phys*. **1996**, *104*, 8821.

(25) Ebata, T.; Hontama, N.; Inokuchi, Y.; Haino, T.; Apra, E.; Xantheas, S. S. *Phys. Chem. Chem. Phys.,* **2010**, *12*, 4569.

(26) Lide, R. D.; CRC HANDBOOK of CHEMISTRY and PHYSICS, 82nd Ed., CRC Press, **2001-2002**, 9-45.

Figure captions

Figure 1. Energy level diagram of the calix[4]alene complexes and the schemes of IR-UV double resonance (IR-UV DR) and IR photodissociation (IRPD) spectroscopy.

Figure 2. Mass selected resonance two-photon ionization spectra formed in supersonic beam of (a) calix[4]alene (C4A) and (b)-(g) its complexes with Ar, N_2, CH_4, C_2H_2, H_2O and NH_3. Lower panel of panel (d): UV-UV hole-burning spectrum of C4A- CH_4 observed by monitoring the band marked by an asterisk.

Figure 3. Red-shift of the S_1-S_0 band origin of the C4A complexes with respect to that of bare C4A versus the polarizability of the guest species.

Figure 4. Left panels: (a) IR-UV DR spectrum of C4A, (b) IR-UV DR spectrum of the C4A-N_2 complex, (c)-(d) Calculated IR spectra of the endo-parallel and endo-perpendicular structures of the C4A-N_2 complex. Right panels: (e) IR-UV DR spectrum of C4A, (f) IR-UV DR spectrum of the C4A-CH_4 complex, (g) Calculated IR spectra of the C4A-N_2 endo-complex.

Figure 5. (a) IR-UV DR spectrum of C4A, (b) IRPD spectrum of the C4A- C_2N_2 complex, (b)-(c) Calculated IR spectra of the endo-perpendicular and exo-structures of the C_2N_2 complex.

Figure 6. (a) IR-UV DR spectrum of C4A, (b) IR-UV DR spectrum of the C4A-NH_3 complex, (c)-(d) calculated IR spectra of the optimized structures of the endo- and exo- C4A-NH_3 complexes, (e) IRPD spectrum of C4A-NH_3.

Figure 7. The optimal structures of (a) parallel C4A-N_2, (b) perpendicular C4A-N_2, (c) endo C4A-CH_4, (d) endo C4A-C_2H_2, (e) exo C4A-C_2H_2, (f) endo C4A-NH_3 and (g) exo C4A-NH_3 obtained at the MP2/aug-cc-pVDZ level of theory.

Table 1. Positions of band origins of C4A and its complexes and their red-shifts with respect to bare C4A.

System	$S_1(0,0)$, cm^{-1}	Shift of band origin, cm^{-1}
C4A	35357	0
C4A-Ar	35312	-45
C4A-CH_4	35289	-68
C4A-N_2	35292	-65
C4A-C_2H_2	35273	-84
C4A-H_2O	35151	-206
C4A-NH_3	35147	-210

Table 2. Relative energies (kJ/mol) of the C4A complexes at different levels of electronic structure theory.

Complex	M05-2X/6-31+G*	MP2/aug-cc-pVDZ
C4A-N_2 / parallel	0	0
perpendicular	3.68	9.95
C4A-C_2H_2 / endo-	0	0
exo-	20.42	48.19
C4A-NH_3 / endo-	0	0
exo-	12.85	34.57

Table 3. Binding energies (kJ/mol) of the endo C4A-M (M=Ar, CH_4, H_2O, N_2, NH_3, C_2H_2) complexes calculated at MP2/aug-cc-pV*n*Z (*n*=D, T, Q) level and experimental estimates. The CCSD(T)/aug-cc-pVDZ binding energies and ratios are shown in parentheses.

Guest	Polarizability (Å^3)	Basis set	Δ*E* (kJ/mol)	Δ*E* (BSSE) (kJ/mol)	Ratio (wrt Ar)	Exp. estimate (kJ/mol)
Ar	1.65	aug-cc-pVDZ	37.50 (29.50)	20.71	1	
		aug-cc-pVTZ	32.53	25.27	1	
		aug-cc-pVQZ	29.18	26.53	1	
		CBS[a)]	26.78	26.78	1	
CH_4	2.59	aug-cc-pVDZ	55.43		1.48	
		aug-cc-pVTZ	41.25		1.27	
		aug-cc-pVQZ	35.33		1.21	
		CBS [a)]	33.47		1.25	
H_2O	1.47	aug-cc-pVDZ	51.58 (45.49)	29.36	1.38 (1.54)	
		aug-cc-pVTZ	43.19	33.39	1.33	
		aug-cc-pVQZ	37.65	34.89	1.29	
		CBS [a)]	33.89	35.15	1.27	37.4 [b)]
N_2	1.76	aug-cc-pVDZ	56.92		1.52	
		aug-cc-pVTZ	45.96		1.41	
		aug-cc-pVQZ	39.54		1.35	
		CBS [a)]	35.98		1.34	
NH_3	2.26	aug-cc-pVDZ	67.08 (56.52)		1.79 (1.92)	
		aug-cc-pVTZ	53.89		1.66	
		aug-cc-pVQZ	48.19		1.65	
		CBS [a)]	46.44		1.73	< 33.5 [c)]
C_2H_2	3.33	aug-cc-pVDZ	76.79		2.05	
		aug-cc-pVTZ	61.83		1.90	
		aug-cc-pVQZ	55.45		1.90	
		CBS [a)]	53.56		2.00	< 33.5 [c)]

[a)] Estimated using $A + B \exp(C\, n^2)$, where *n* is the cardinal number (*n*=2, 3, 4) of the aug-cc-pV*n*Z basis set. [b)] Reference (15). [c)] Estimated from the lowest IR band appeared in the IRPD spectra of Figures 5 and 6.

Figure 1. Energy level diagram of the calix[4]alene complexes and the schemes of IR-UV double resonance (IR-UV DR) and IR photodissociation (IRPD) spectroscopy.

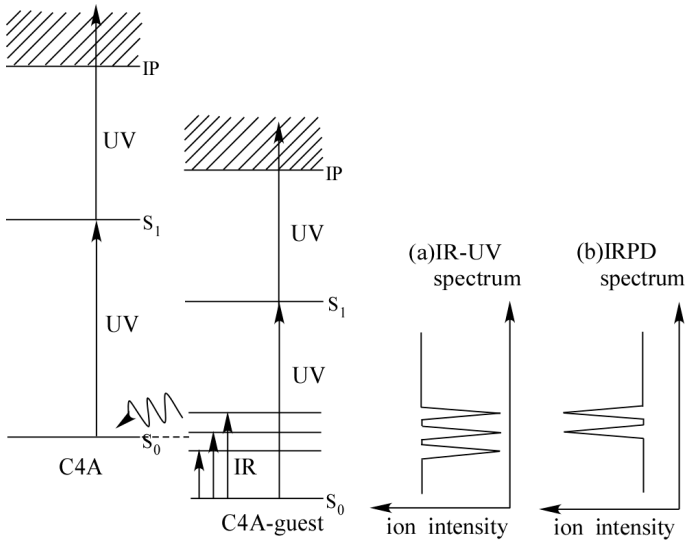

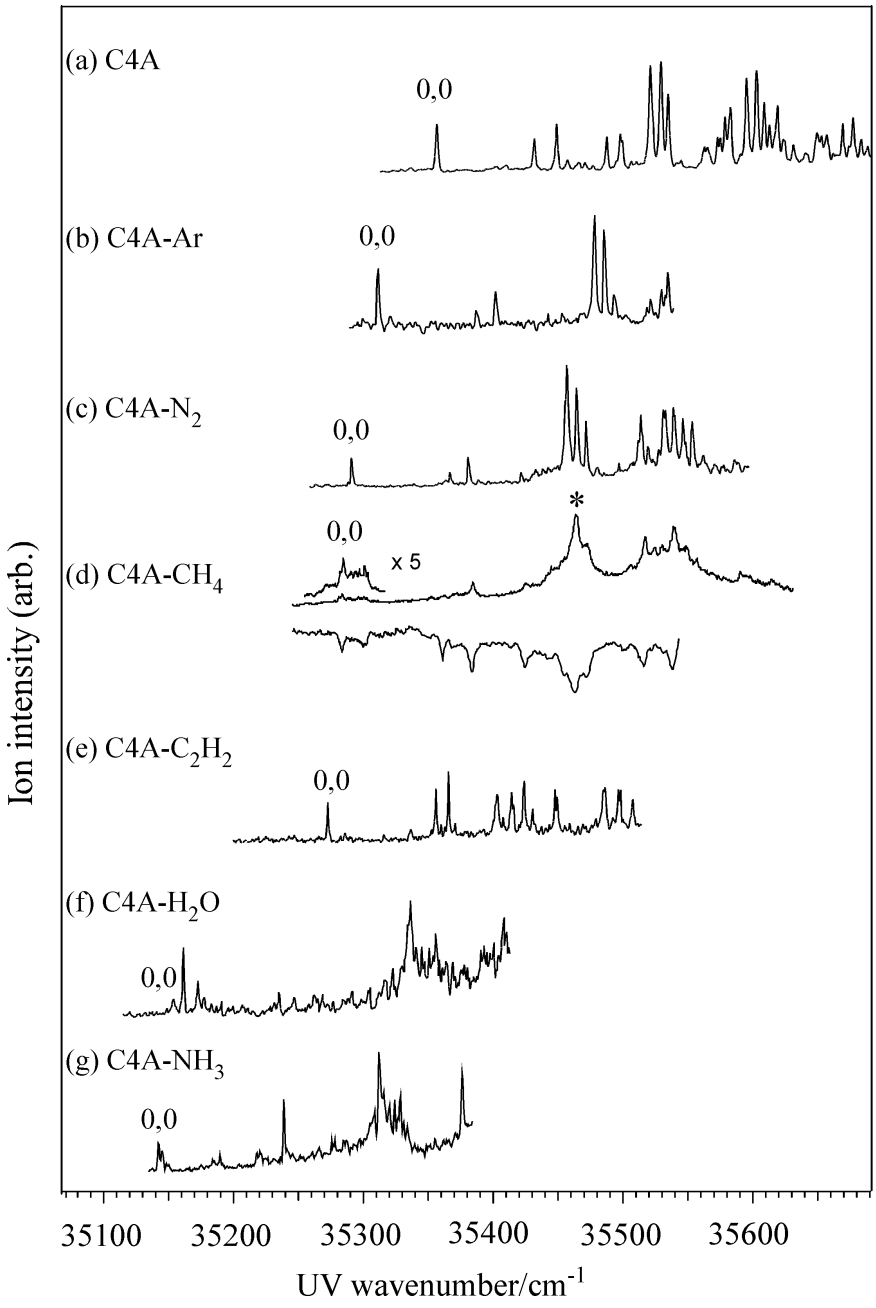

Figure 2. Mass selected resonance two-photon ionization spectra formed in supersonic beam of (a) calix[4]alene (C4A) and (b)-(g) its complexes with Ar, N_2, CH_4, C_2H_2, H_2O and NH_3. Lower panel of panel (d): UV-UV hole-burning spectrum of C4A- CH_4 observed by monitoring the band marked by an asterisk.

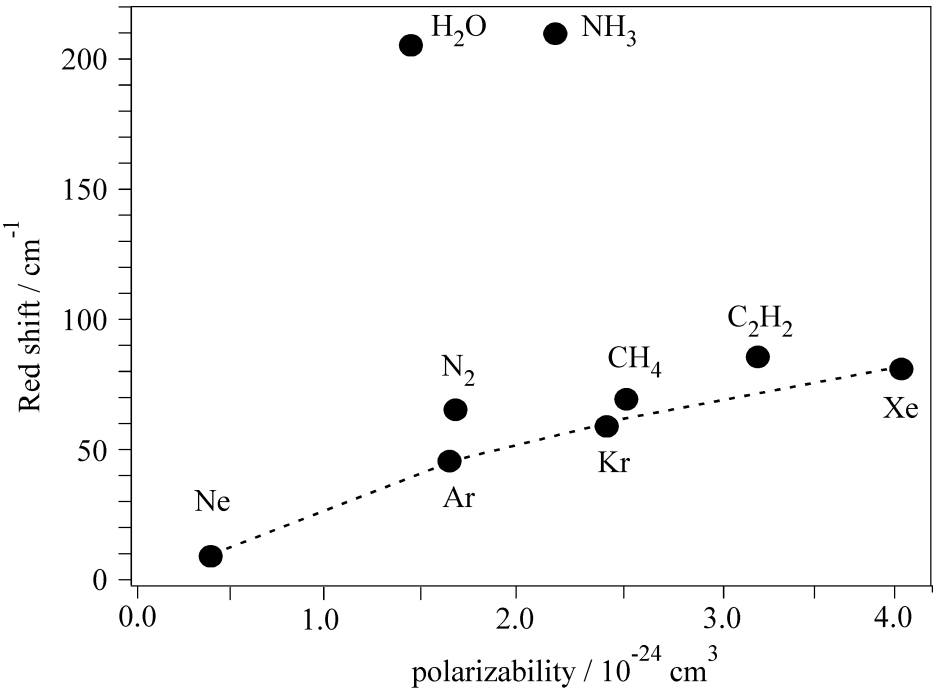

Figure 3. Red-shift of the S_1-S_0 band origin of the C4A complexes with respect to that of bare C4A versus the polarizability of the guest species.

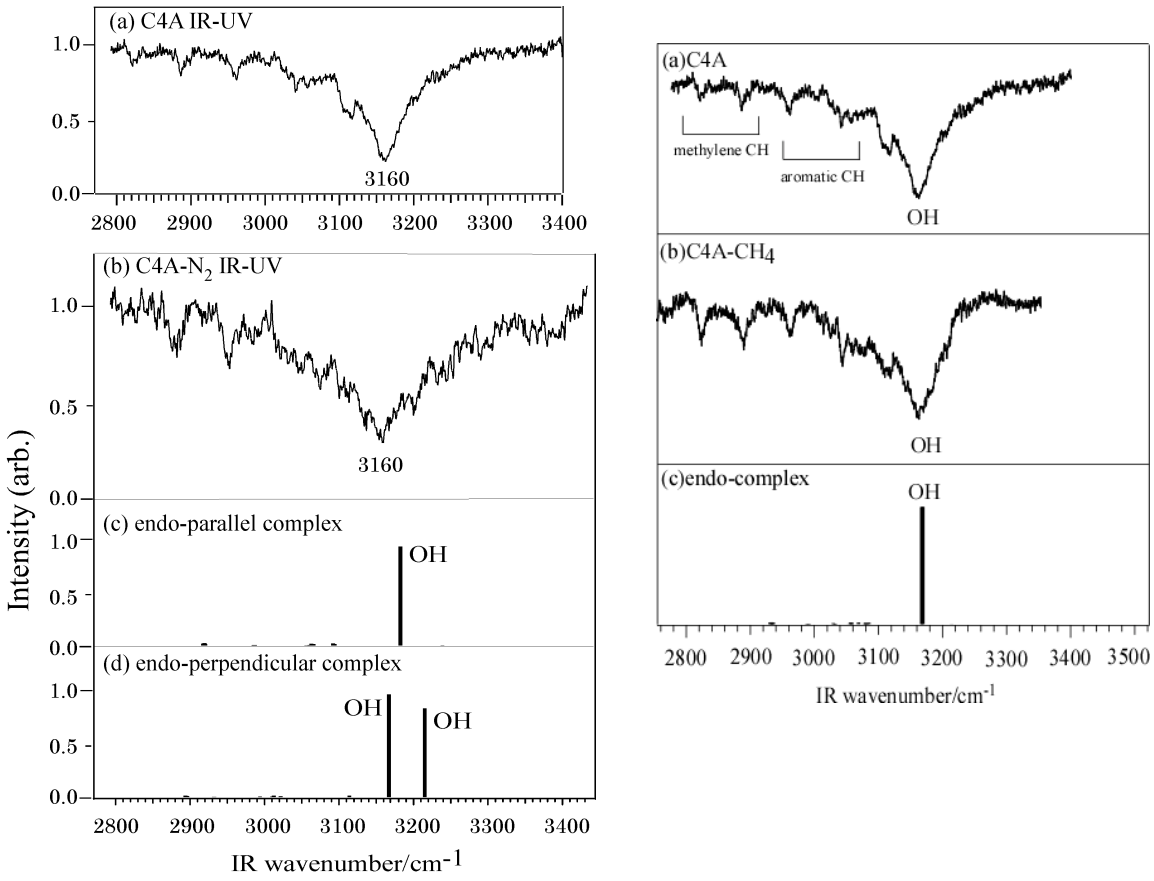

Figure 4. Left panels: (a) IR-UV DR spectrum of C4A, (b) IR-UV DR spectrum of the C4A-N_2 complex, (c)-(d) Calculated IR spectra of the endo-parallel and endo-perpendicular structures of the C4A-N_2 complex. Right panels: (e) IR-UV DR spectrum of C4A, (f) IR-UV DR spectrum of the C4A-CH_4 complex, (g) Calculated IR spectra of the C4A-N_2 endo-complex.

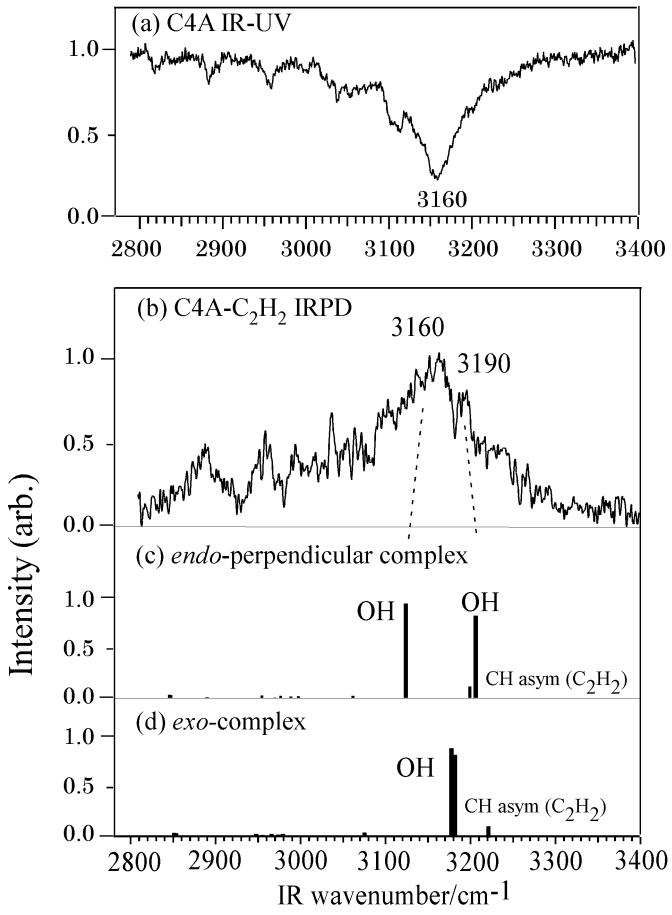

Figure 5. (a) IR-UV DR spectrum of C4A, (b) IRPD spectrum of the C4A- C_2H_2 complex, (b)-(c) Calculated IR spectra of the endo-perpendicular and exo-structures of the C_2H_2 complex.

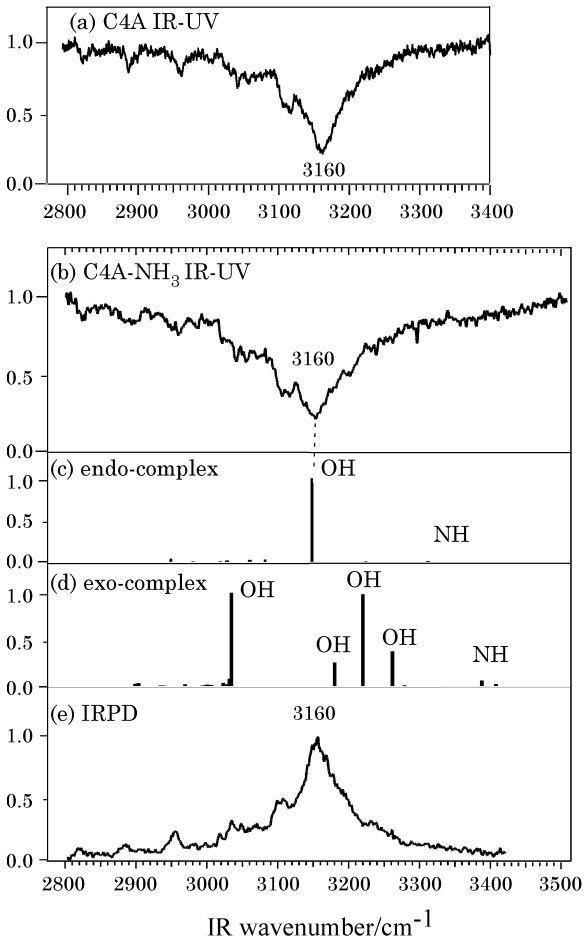

Figure 6. a) IR-UV DR spectrum of C4A, (b) IR-UV DR spectrum of the C4A-NH_3 complex, (c)-(d) calculated IR spectra of the optimized structures of the endo- and exo- C4A-NH_3 complexes, (e) IRPD spectrum of C4A-NH_3.

side view top view

(b) *perpend*

+9

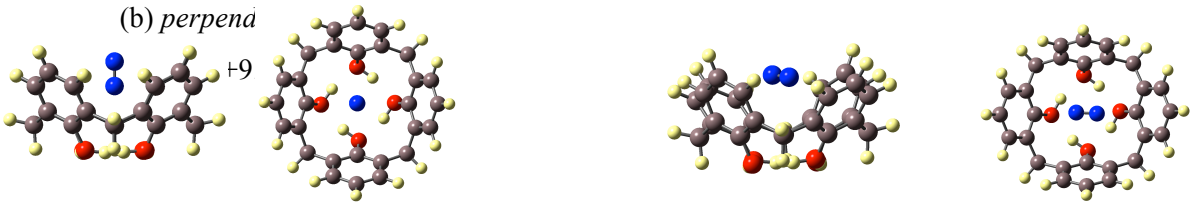

v top view

endo-C4A-CH_4

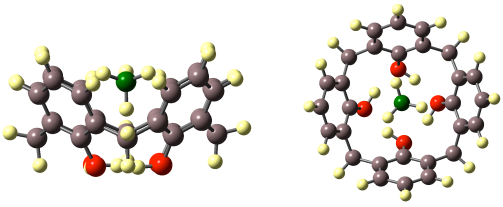

side view bottom view

(e) *exo*

+

side view bottom view

(g) *exo*

+

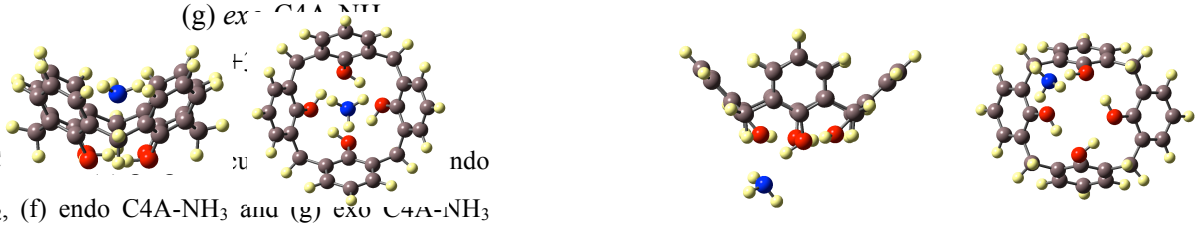

a) parallel C ndo

o C4A-C_2H_2, (f) endo C4A-NH_3 and (g) exo C4A-NH_3

l of theory.